



Cite this: *Chem. Commun.*, 2020, 56, 9449

Received 11th May 2020,  
Accepted 10th July 2020

DOI: 10.1039/d0cc03385e

[rsc.li/chemcomm](http://rsc.li/chemcomm)

A mononuclear cobalt(III)-bis(tert-butyperoxo) adduct ( $\text{Co}^{\text{III}}-(\text{OO}^{\text{t}}\text{Bu})_2$ ) bearing a tetraazamacrocyclic ligand was synthesized and characterized using various physicochemical methods, such as X-ray, UV-vis, ESI-MS, EPR, and NMR analyses. The crystal structure of the  $\text{Co}^{\text{III}}-(\text{OO}^{\text{t}}\text{Bu})_2$  complex clearly showed that two  $\text{OO}^{\text{t}}\text{Bu}$  ligands bound to the equatorial position of the cobalt(III) center. Kinetic studies and product analyses indicate that the  $\text{Co}^{\text{III}}-(\text{OO}^{\text{t}}\text{Bu})_2$  intermediate exhibits nucleophilic oxidative reactivity toward external organic substrates.

Transition metal-alkylperoxo (M-OOR) species play an important role in oxidation reactions such as industrial and biological catalytic oxidation.<sup>1–6</sup> In industrial processes, M-OOR intermediates, such as  $\text{Co}^{\text{III}}\text{-OOR}$  complexes, were proposed as key intermediates in hydrocarbon catalytic oxidation under harsh conditions.<sup>1,7</sup> Mononuclear nonheme M-OOR complexes have been suggested to play a significant role in the oxidation reaction of metalloenzyme systems (e.g., lipoxygenase and homoprotocatechuate 2,3-dioxygenase).<sup>8,9</sup> Biomimetic studies of M-OOR complexes enabled catalysts to be developed that produce high value-added organic products under mild conditions.

Mononuclear heme and nonheme first-row M-OOR intermediates (M = Mn, Fe, Co, Ni, and Cu) have been investigated as model complexes for the active sites of metalloenzymes.<sup>2,5,6,10–13</sup> A number of M-OOR complexes were mainly studied in the investigation of electrophilic reactions (e.g., oxygen and hydrogen atom transfer reaction).<sup>14–25</sup> It has been reported that the reaction proceeds *via* the  $\bullet\text{OOR}$  and  $\bullet\text{OR}$  radicals from decomposition of the M-OOR species.<sup>1</sup> However, only a few examples of nucleophilic reactivity with M-OOR intermediates (M = Fe, Ni, and Cu) have been reported.<sup>19,20,23</sup>

Department of Emerging Materials Science, DGIST, Daegu 42988, Korea.

E-mail: [jaeheung@dgist.ac.kr](mailto:jaeheung@dgist.ac.kr)

† Electronic supplementary information (ESI) available: Synthesis and characterization data and kinetic details. CCDC 1906994–1906996. For ESI and crystallographic data in CIF or other electronic format see DOI: 10.1039/d0cc03385e

‡ These authors contributed equally to this work.

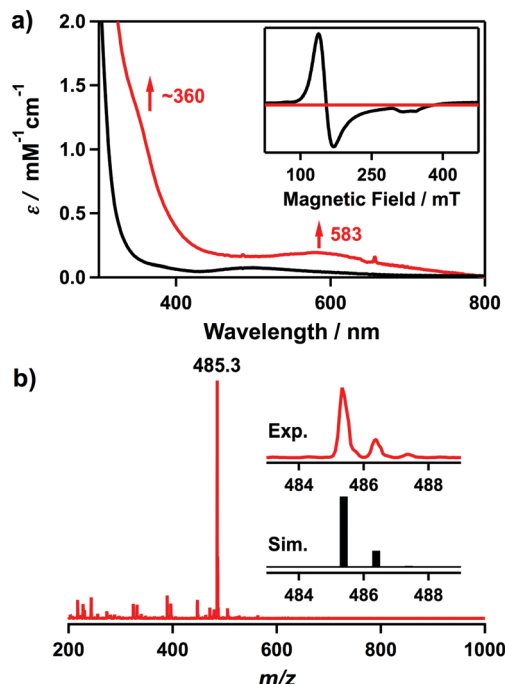
## Nucleophilic reactivity of a mononuclear cobalt(III)-bis(tert-butylperoxo) complex†

Bongki Shin, ‡ Younwoo Park, ‡ Donghyun Jeong and Jaeheung Cho \*  
 \* To whom correspondence should be addressed.

In the Sharpless-Katsuki epoxidation,  $\text{Ti}-(\text{OOR})_n$  ( $n = 1\text{--}4$ ) species were proposed as reactive intermediates.<sup>26,27</sup> Furthermore, in the formation of  $\text{Fe}-\text{OO}^{\text{t}}\text{Bu}$  complexes,  $\text{Fe}-(\text{OO}^{\text{t}}\text{Bu})_2$  species,  $[\text{Fe}^{\text{III}}(\text{TPP})(\text{OO}^{\text{t}}\text{Bu})_2]^-$  (TPP = 5,10,15,20-tetraphenylporphyrinate) and  $[\text{Fe}^{\text{III}}(\text{BPMCN})(\text{OO}^{\text{t}}\text{Bu})(\text{HOO}^{\text{t}}\text{Bu})]^{2+}$  (BPMCN =  $N,N'$ -bis(2-pyridylmethyl- $N,N'$ -dimethyl-*trans*-1,2-diaminocyclohexane)) adducts, have been proposed as short-lived intermediates.<sup>28–31</sup> However, definitive evidence of bis(alkylperoxo) binding first-row transition metal compounds has not been reported yet. In this work, we report a fully characterized  $\text{Co}^{\text{III}}-(\text{OO}^{\text{t}}\text{Bu})_2$  complex bearing a tetraazamacrocyclic ligand,  $[\text{Co}^{\text{III}}(\text{Me}_3\text{-TPADP})(\text{OO}^{\text{t}}\text{Bu})_2]^{+}$  (2,  $\text{Me}_3\text{-TPADP}$  = 3,6,9-trimethyl-3,6,9-triaza-1(2,6)-pyridinacyclodecaphane). Intermediate 2 was investigated in nucleophilic reactions such as aldehyde oxidation. Only one of the two  $\text{OO}^{\text{t}}\text{Bu}$  ligands in 2 is able to oxidize external substrates. In order to compare the structure and the reactivity of an alkylperoxo and bis(alkylperoxo) binding cobalt species,  $\text{Co}^{\text{III}}-(\text{OO}^{\text{t}}\text{Bu})(\text{X})$  complexes,  $[\text{Co}^{\text{III}}(\text{Me}_3\text{-TPADP})(\text{OO}^{\text{t}}\text{Bu})(\text{X})]^{+}$  (X = N<sub>3</sub> for 4, NCS for 5), were prepared as well.

The cobalt(II) starting complex,  $[\text{Co}^{\text{II}}(\text{Me}_3\text{-TPADP})(\text{CH}_3\text{CN})_2]^{2+}$  (1), was synthesized by using a published method.<sup>32</sup> When 10 equiv. of *tert*-butyl hydroperoxide ( $\text{BuOOH}$ ) was added to 1 in the presence of 2 equiv. of triethylamine (TEA) in  $\text{CH}_3\text{CN}$  at 25 °C, the  $\text{Co}^{\text{III}}-(\text{OO}^{\text{t}}\text{Bu})_2$  adduct,  $[\text{Co}^{\text{III}}(\text{Me}_3\text{-TPADP})(\text{OO}^{\text{t}}\text{Bu})_2]^{+}$  (2), was generated and the solution color changed from purple to dark green (Scheme S1, ESI†). Intermediate 2 is thermally metastable in  $\text{CH}_3\text{CN}$  at 25 °C, which allowed us to use it for characterization and reactivity studies.

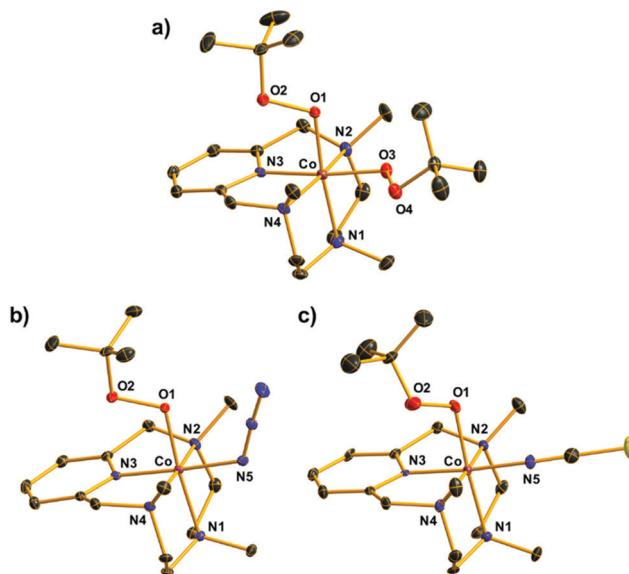
The UV-vis spectrum of 2 in  $\text{CH}_3\text{CN}$  at 25 °C shows electronic absorption bands at  $\lambda_{\text{max}} = \sim 360$  ( $\varepsilon = 1100 \text{ M}^{-1} \text{ cm}^{-1}$ ) and 583 nm ( $\varepsilon = 190 \text{ M}^{-1} \text{ cm}^{-1}$ ) (Fig. 1a). Electrospray ionization mass spectrometry (ESI-MS) analysis of 2 exhibits a prominent ion peak at  $m/z$  485.3, whose mass and isotope distribution pattern correspond to  $[\text{Co}^{\text{III}}(\text{Me}_3\text{-TPADP})(\text{OO}^{\text{t}}\text{Bu})_2]^{+}$  (calcd  $m/z$  485.3) (Fig. 1b). The X-band electron paramagnetic resonance (EPR) silence (Fig. 1a, inset) and <sup>1</sup>H NMR spectral features (Fig. S1, ESI†) in the diamagnetic region confirm that complex 2 is a low-spin  $S = 0$  cobalt(III) species.



**Fig. 1** (a) UV-vis spectra of  $[\text{Co}^{\text{II}}(\text{Me}_3\text{-TPADP})(\text{CH}_3\text{CN})_2]^{2+}$  (**1**) (the black line) and  $[\text{Co}^{\text{III}}(\text{Me}_3\text{-TPADP})(\text{OO}^{\text{t}}\text{Bu})_2]^{+}$  (**2**) (the red line) in  $\text{CH}_3\text{CN}$  at 25 °C.<sup>32</sup> Inset shows the X-band EPR spectra of **1** (the black line) in frozen  $\text{CH}_3\text{CN}$  at 5 K and **2** (the red line) in frozen  $\text{CH}_3\text{CN}$  at 113 K.<sup>32</sup> The parameters for the measurement of **2**: microwave power = 1.0 mW, frequency = 9.176 GHz, sweep width = 0.40 T, and modulation amplitude = 0.60 mT. (b) ESI-MS of **2** in  $\text{CH}_3\text{CN}$  at -40 °C. Insets show experimental (upper) and simulated (lower) isotope distribution patterns.

The X-ray crystal structure of  $[\text{Co}^{\text{III}}(\text{Me}_3\text{-TPADP})(\text{OO}^{\text{t}}\text{Bu})_2](\text{BPh}_4)(\text{Et}_2\text{O})$  (**2-BPh<sub>4</sub>-Et<sub>2</sub>O**) revealed a distorted octahedral geometry where two *tert*-butyl peroxide ligands coordinate to the cobalt(III) center in the *cis* positions (Fig. 2a). To the best of our knowledge, this is the first crystal structure of a mononuclear  $\text{Co}^{\text{III}}\text{-}(\text{OO}^{\text{t}}\text{Bu})_2$  complex. The average Co–O (1.8590 Å) and O–O (1.4757 Å) bond distances of **2** are comparable to those of the  $\text{Co}^{\text{III}}\text{-OO}^{\text{t}}\text{Bu}$  complexes (Table S2, ESI†).<sup>1,33</sup>

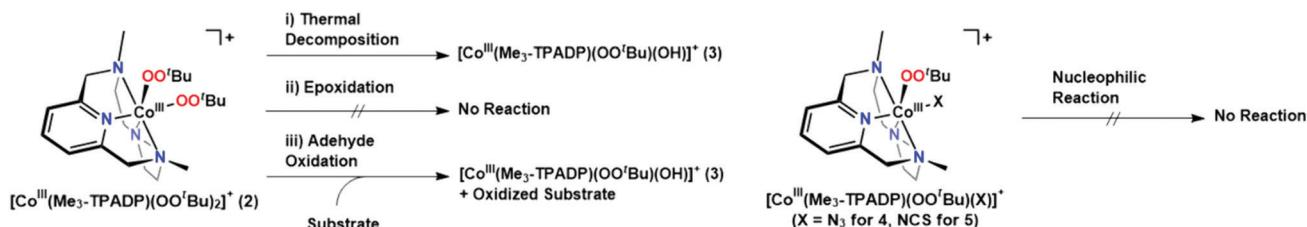
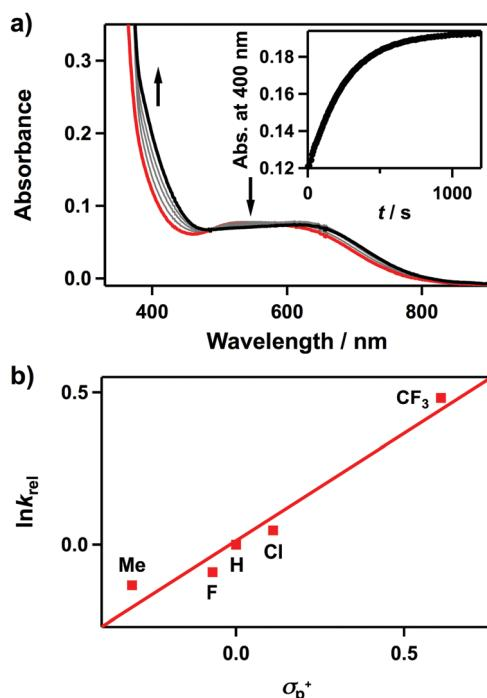
Thermal decomposition of **2** produced a  $\text{Co}^{\text{III}}\text{-}(\text{OO}^{\text{t}}\text{Bu})(\text{OH})$  complex,  $[\text{Co}^{\text{III}}(\text{Me}_3\text{-TPADP})(\text{OO}^{\text{t}}\text{Bu})(\text{OH})]^{+}$  (**3**), in  $\text{CH}_3\text{CN}$  at 25 °C (Fig. S2, ESI†).<sup>34</sup> Formation of **3** was confirmed by cold spray ionization spectrometry (CSI-MS). The CSI-MS spectrum of **3** shows a prominent signal at  $m/z$  413.17 (calcd  $m/z$  413.20) (Fig. S3, ESI†). Upon adding isotopically labeled  $\text{H}_2^{18}\text{O}$  and  $\text{D}_2\text{O}$  into the solution of **3**, mass peaks at 415.21 and 414.22 corresponding to  $[\text{Co}^{\text{III}}(\text{Me}_3\text{-TPADP})(\text{OO}^{\text{t}}\text{Bu})(^{18}\text{OH})]^{+}$  (calcd  $m/z$  415.20) and  $[\text{Co}^{\text{III}}(\text{Me}_3\text{-TPADP})(\text{OO}^{\text{t}}\text{Bu})(\text{OD})]^{+}$  (calcd  $m/z$  414.20), respectively, were observed (Fig. S3, ESI†, the inset). These mass shifts demonstrate that **3** contains a hydroxide ligand. In a previous study, the  $\text{Fe}-(\text{OO}^{\text{t}}\text{Bu})_2$  species was also proposed as a precursor of the  $\text{Fe}-(\text{OO}^{\text{t}}\text{Bu})$  species.<sup>29</sup> Tajima *et al.* insisted that  $[\text{Fe}^{\text{III}}(\text{TPP})(\text{OO}^{\text{t}}\text{Bu})_2]^{-}$ , generated by adding an excess amount of sodium methoxide ( $\text{NaOCH}_3$ ) and  $^{\text{t}}\text{BuOOH}$  to the  $[\text{Fe}^{\text{III}}(\text{TPP})]^{+}$  solution, reacted with additional  $\text{NaOCH}_3$ , affording the formation of the  $[\text{Fe}^{\text{III}}(\text{TPP})(\text{OO}^{\text{t}}\text{Bu})(\text{OCH}_3)]^{-}$  species.<sup>29</sup>



**Fig. 2** ORTEP plots of the (a)  $\text{Co}^{\text{III}}\text{-}(\text{OO}^{\text{t}}\text{Bu})_2$  complex,  $[\text{Co}^{\text{III}}(\text{Me}_3\text{-TPADP})(\text{OO}^{\text{t}}\text{Bu})_2]^{+}$  (**2**), and  $\text{Co}^{\text{III}}\text{-}(\text{OO}^{\text{t}}\text{Bu})(\text{X})$  complexes,  $[\text{Co}^{\text{III}}(\text{Me}_3\text{-TPADP})(\text{OO}^{\text{t}}\text{Bu})(\text{X})]^{+}$  (X = (b)  $\text{N}_3$  (**4**), (c) NCS (**5**)), with thermal ellipsoids drawn at the 30% probability level. Hydrogen atoms are omitted for clarity.

We then investigated the electrophilic and nucleophilic reactivities of **2**. The electrophilic reaction of **2** was performed by using styrene and 2,3-dimethyl-2-butene. Upon addition of substrates to the solution of **2** in  $\text{CH}_3\text{CN}$  at 10 °C, the intermediate remained intact without showing specific UV-vis spectral changes, and product analysis of these reaction solutions did not show oxidized products (Scheme 1). In contrast, the nucleophilic reactivity of **2** was observed in the oxidation of aldehydes (Scheme 1). Upon the addition of benzaldehyde to **2** in  $\text{CH}_3\text{CN}$  at 15 °C, the characteristic absorption band of **2** disappeared with a pseudo-first-order decay (Fig. 3a, the inset and Table S3, ESI†). The product analysis of the reaction solution revealed that benzoic acid (95(1)% was produced in the oxidation of benzaldehyde (Scheme S2, ESI†). In addition, the cobalt(II)-benzoato complex,  $[\text{Co}^{\text{II}}(\text{Me}_3\text{-TPADP})(\text{C}_6\text{H}_5\text{COO})]^{+}$ , was generated after the reaction was completed (Fig. S7, ESI† for CSI-MS analysis). The reactivity of **2** was further investigated with *para*-substituted benzaldehydes, *para*-X-Ph-CHO (X = Me, F, Cl, and  $\text{CF}_3$ ) (Table S3, ESI†). The Hammett plot of the pseudo-first-order rate constants *versus*  $\sigma_p^+$  gave a  $\rho$  value of 0.7(1) (Fig. 3b). The positive  $\rho$  value indicates that **2** has nucleophilic character. The reactivity of **2** was further examined by using primary (1-pentanal for 1°-CHO), secondary (2-methylbutanal for 2°-CHO), and tertiary (pivalaldehyde for 3°-CHO) aldehydes, and the observed reactivity order of 1°-CHO > 2°-CHO > 3°-CHO supports the nucleophilic character of **2** as well (Fig. S8, ESI†). Product analyses of the resulting solutions revealed that pentanoic acid (94(3)%), 2-methylbutanoic acid (94(4)%), and 2,2-dimethylpropanoic acid (94(1)% were produced in the oxidation of 1-pentanal, 2-methylbutanal, and pivalaldehyde, respectively (Table S4, ESI†).

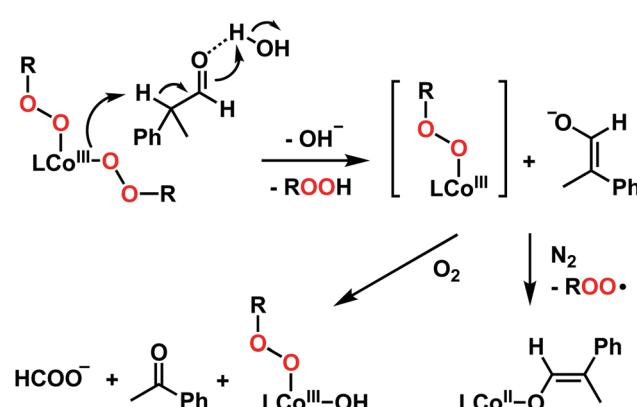
Upon the addition of 2-phenylpropionaldehyde (2-PPA) to **2** in  $\text{CH}_3\text{CN}$  at 25 °C under aerobic conditions, the UV-vis absorption

Scheme 1 Overall electrophilic and nucleophilic reactivities of **2**, **4** and **5**.Fig. 3 Reactions of  $[\text{Co}^{\text{III}}(\text{Me}_3\text{-TPADP})(\text{OO}'\text{Bu})_2]^+$  (**2**) with benzaldehyde in  $\text{CH}_3\text{CN}/\text{MeOH}$  ( $v/v = 3:1$ ). (a) UV-vis spectral changes of **2** (0.5 mM) upon addition of 200 equiv. of benzaldehyde at  $15^\circ\text{C}$ . Inset shows the time course of the absorbance at 400 nm. (b) Hammett plot of  $\ln k_{\text{rel}}$  against  $\sigma_p^+$  of *para*-substituted benzaldehydes. The  $k_{\text{rel}}$  values were calculated by dividing  $k_{\text{obs}}$  of *para*-X-Ph-CHO ( $X = \text{Me, F, H, Cl, and } \text{CF}_3$ ) by  $k_{\text{obs}}$  of benzaldehyde at  $15^\circ\text{C}$ .

band of **2** slightly changed with isosbestic points at 390 and 452 nm, which follows a pseudo-first-order decay profile (Fig. S9, ESI<sup>†</sup>). The pseudo-first-order rate constants increased proportionally with the 2-PPA concentration, giving a second-order rate constant ( $k_2$ ) of  $4.1(3) \times 10^{-1} \text{ M}^{-1} \text{ s}^{-1}$  at  $25^\circ\text{C}$  (Fig. S10a, ESI<sup>†</sup>). After the reaction of **2** with 2-PPA, product analysis revealed that acetophenone (95(1)% was produced as a final product. The CSI-MS spectrum of the reaction solution revealed the formation of **3** and a small amount of cobalt(II)-formato species was also detected under an inert atmosphere (Fig. S11, ESI<sup>†</sup>). The temperature dependence of the  $k_2$  values was examined in the range of 273–298 K, where a linear Eyring plot was obtained with the activation parameters of  $\Delta H^\ddagger = 11(1) \text{ kcal mol}^{-1}$  and  $\Delta S^\ddagger = -22(3) \text{ cal mol}^{-1} \text{ K}^{-1}$  (Fig. S10b, ESI<sup>†</sup>). The observed negative entropy value and the second-order kinetics suggest that the oxidation of 2-PPA by **2** is performed through a bimolecular mechanism.

Interestingly, the same reaction performed under a  $\text{N}_2$  atmosphere gives different products. The reaction of **2** with 2-PPA under  $\text{N}_2$  in  $\text{CH}_3\text{CN}$  at  $25^\circ\text{C}$  gave a new absorption band at 480 nm (Fig. S12, ESI<sup>†</sup>). By analysing the resulting solution with CSI-MS, we found that a cobalt(II)-enolate complex,  $[\text{Co}^{\text{II}}(\text{Me}_3\text{-TPADP})(\text{OCH}=\text{C}(\text{Me})\text{Ph})]^+$ , was formed as a decomposed product (Fig. S13, ESI<sup>†</sup>). The product analysis of the reaction solution indicated that trace amounts of acetophenone were produced (<1%) after the reaction. When the cobalt(II)-enolate complex was exposed to  $\text{O}_2$ , a cobalt(II)-formato complex was obtained as a major product, as observed by CSI-MS (Fig. S14, ESI<sup>†</sup>). These results are very similar to Tolman's recent mechanism of the aldehyde deformylation pathway *via* a copper(II)-enolate species.<sup>35</sup> Based on the kinetic studies and product analyses under  $\text{N}_2$  and  $\text{O}_2$ , the possible reaction mechanisms for 2-PPA oxidation by **2** are summarized in Scheme 2. The reaction of **2** and 2-PPA in the presence of water afforded enolate and a putative cobalt(III)-(OO'<sup>+</sup>Bu) species through  $\alpha$ -deprotonation of 2-PPA by one of the alkylperoxides of **2**. The putative cobalt(III)-(OO'<sup>+</sup>Bu) species decomposed to the cobalt(II)-enolate complex under  $\text{N}_2$ . In the presence of  $\text{O}_2$ , the enolate is oxidized to acetophenone, and complex **3** is produced as a final product.

In the aldehyde oxidation, only one  $\text{OO}'\text{Bu}$  ligand in **2** was able to participate in the oxidation of 2-PPA (Scheme 1). To compare the reactivity properties of  $\text{Co}^{\text{III}}-(\text{OO}'\text{Bu})$  and  $\text{Co}^{\text{III}}-(\text{OO}'\text{Bu})_2$  complexes,  $\text{Co}^{\text{III}}-(\text{OO}'\text{Bu})(\text{X})$  complexes,  $[\text{Co}^{\text{III}}(\text{Me}_3\text{-TPADP})(\text{OO}'\text{Bu})(\text{X})]^+$  ( $\text{X} = \text{N}_3$  for **4**, NCS for **5**), were synthesized. **4** and **5** were prepared by adding 1.1 equiv. of  $\text{NaX}$  ( $\text{X} = \text{N}_3$ , NCS) to the reaction solution of **1** in  $\text{CH}_3\text{CN}$  at  $25^\circ\text{C}$  and then 5 equiv.

Scheme 2 Proposed reaction pathways of **2** with 2-PPA under  $\text{N}_2$  and  $\text{O}_2$  ( $\text{L} = \text{Me}_3\text{-TPADP}$ ,  $\text{R} = \text{Bu}'$ ).

of  $^t\text{BuOOH}$  and 2 equiv. of TEA were added (Scheme S1, ESI $\dagger$ ). Characterization of **4** and **5** was performed by UV-vis, ESI-MS, EPR, and  $^1\text{H}$  NMR analyses (Experimental section and Fig. S15–S19, ESI $\dagger$ ).

The single crystals of **4** and **5** revealed a similar distorted octahedral geometry to that of **2** in which one  $\text{OO}'\text{Bu}$  ligand bound to the cobalt(III) center was located in the *trans* position of the amine group and the other anionic monodentate ligand, X, was located in the *trans* position of the pyridine ring (Fig. 2b and c). These data clearly indicate that the  $\text{OO}'\text{Bu}$  ligand in the *trans* position of the pyridine ring in **2** was substituted with an anionic ligand in **3** and **4**. The Co–O1 bond distances (1.862(3) Å for **4**, 1.880(4) Å for **5**) and O1–O2 bond distances (1.479(4) Å for **4**, 1.430(6) Å for **5**) were within the range of those of the reported  $\text{Co}^{\text{III}}\text{–OO}'\text{Bu}$  complexes and similar to those of **2** (Table S2, ESI $\dagger$ ).<sup>1,33</sup>

In the reactions of **4** and **5** with 2-PPA, we could not observe any change in the UV-vis spectra. Based on the reactivity and structural comparison of **2**, **4**, and **5**, the reaction site of **2** is presumed to be the  $\text{OO}'\text{Bu}$  ligand in the *trans* position of the pyridine ring. Further theoretical calculations on the detailed reaction mechanism of **2** with substrates are underway and will clarify the reaction site of **2**.

In conclusion, we have synthesized and characterized a mononuclear  $\text{Co}^{\text{III}}\text{–}(\text{OO}'\text{Bu})_2$  intermediate,  $[\text{Co}^{\text{III}}(\text{Me}_3\text{-TPADP})(\text{OO}'\text{Bu})_2]^+$  (**2**), with various physicochemical methods including UV-vis, ESI-MS, EPR, X-ray, and NMR analyses. In the kinetic studies, under mild conditions, one of the two  $\text{OO}'\text{Bu}$  ligands in **2** is capable of performing a nucleophilic reaction (*i.e.*, aldehyde oxidation). A  $\text{Co}^{\text{III}}\text{–}(\text{OO}'\text{Bu})(\text{OH})$  complex, **3**, was generated by thermal decomposition of **2** and/or deformylation reaction of 2-PPA by **2** in the presence of  $\text{O}_2$ . Furthermore,  $\text{Co}^{\text{III}}\text{–}(\text{OO}'\text{Bu})$  complexes,  $[\text{Co}^{\text{III}}(\text{Me}_3\text{-TPADP})(\text{OO}'\text{Bu})(\text{X})]^+$  ( $\text{X} = \text{N}_3$  for **4**, NCS for **5**), which have a  $\text{OO}'\text{Bu}$  ligand in the *trans* position of the amine group were prepared, and **4** and **5** did not undergo aldehyde oxidation.

This research was supported by the NRF (2019R1A2C2086249 and 2018R1A5A1025511) and the Ministry of Science, ICT and Future Planning (CGRC 2016M3D3A01913243) of Korea.

## Conflicts of interest

The authors declare no competing financial interest.

## Notes and references

- 1 F. A. Chavez and P. K. Mascharak, *Acc. Chem. Res.*, 2000, **33**, 539–545.
- 2 S. Hikichi, M. Akita and Y. Moro-Oka, *Coord. Chem. Rev.*, 2000, **198**, 61–87.
- 3 M. Costas, M. P. Mehn, M. P. Jensen and L. Que, Jr., *Chem. Rev.*, 2004, **104**, 939–986.

- 4 B. de Bruin, P. H. M. Budzelaar and A. W. Gal, *Angew. Chem., Int. Ed.*, 2004, **43**, 4142–4157.
- 5 S. Itoh, *Acc. Chem. Res.*, 2015, **48**, 2066–2074.
- 6 A. T. Fiedler and A. A. Fischer, *J. Biol. Inorg. Chem.*, 2017, **22**, 407–424.
- 7 J. F. Black, *J. Am. Chem. Soc.*, 1978, **100**, 527–535.
- 8 E. G. Kovaleva and J. D. Lipscomb, *Science*, 2007, **316**, 453–457.
- 9 E. Skrzypeczak-Jankun, R. A. Bross, R. T. Carroll, W. R. Dunham and M. O. Funk, Jr., *J. Am. Chem. Soc.*, 2001, **123**, 10814–10820.
- 10 H. Komatsuzaki, N. Sakamoto, M. Satoh, S. Hikichi, M. Akita and Y. Moro-oka, *Inorg. Chem.*, 1998, **37**, 6554–6555.
- 11 S. Hong, Y.-M. Lee, K.-B. Cho, M. S. Seo, D. Song, J. Yoon, R. Garcia-Serres, M. Clémancey, T. Ogura, W. Shin, J.-M. Latour and W. Nam, *Chem. Sci.*, 2014, **5**, 156–162.
- 12 J. A. Kovac, *Acc. Chem. Res.*, 2015, **48**, 2744–2753.
- 13 M. Sankaralingam, Y.-M. Lee, W. Nam and S. Fukuzumi, *Coord. Chem. Rev.*, 2018, **365**, 41–59.
- 14 N. Kitajima, T. Katayama, K. Fujisawa, Y. Iwata and Y. Morooka, *J. Am. Chem. Soc.*, 1993, **115**, 7872–7873.
- 15 J. Kim, E. Larka, E. C. Wilkinson and L. Que, Jr., *Angew. Chem., Int. Ed. Engl.*, 1995, **34**, 2048–2051.
- 16 M. S. Seo, T. Kamachi, T. Kouno, K. Murata, M. J. Park, K. Yoshizawa and W. Nam, *Angew. Chem., Int. Ed.*, 2007, **46**, 2291–2294.
- 17 S. Gosiewska, H. P. Permentier, A. P. Bruins, G. van Koten and R. J. M. Gebbink, *Dalton Trans.*, 2007, 3365–3368.
- 18 A. Kunishita, H. Ishimaru, S. Nakashima, T. Ogura and S. Itoh, *J. Am. Chem. Soc.*, 2008, **130**, 4244–4245.
- 19 S. Hikichi, H. Okuda, Y. Ohzu and M. Akita, *Angew. Chem., Int. Ed.*, 2009, **48**, 188–191.
- 20 J. Stasser, F. Namuswe, G. D. Kasper, Y. Jiang, C. M. Krest, M. T. Green, J. Penner-Hahn and D. P. Goldberg, *Inorg. Chem.*, 2010, **49**, 9178–9190.
- 21 T. Tano, M. Z. Ertem, S. Yamaguchi, A. Kunishita, H. Sugimoto, N. Fujieda, T. Ogura, C. J. Cramer and S. Itoh, *Dalton Trans.*, 2011, **40**, 10326–10336.
- 22 S. Paria, T. Ohta, Y. Morimoto, T. Ogura, H. Sugimoto, N. Fujieda, K. Goto, K. Asano, T. Suzuki and S. Itoh, *J. Am. Chem. Soc.*, 2015, **137**, 10870–10873.
- 23 B. Kim, D. Jeong and J. Cho, *Chem. Commun.*, 2017, **53**, 9328–9331.
- 24 T. Abe, Y. Morimoto, K. Mieda, H. Sugimoto, N. Fujieda, T. Ogura and S. Itoh, *J. Inorg. Biochem.*, 2017, **177**, 375–383.
- 25 J. Lewiński, Z. Ochal, E. Bojarski, E. Tratkiewicz, I. Justyniak and J. Lipkowski, *Angew. Chem., Int. Ed.*, 2003, **42**, 4643–4646.
- 26 T. Katsuki and K. B. Sharpless, *J. Am. Chem. Soc.*, 1980, **102**, 5974–5976.
- 27 D. E. Babushkin and E. P. Talsi, *J. Mol. Catal. A: Chem.*, 2003, **200**, 165–175.
- 28 M. Rivera, G. A. Caignan, A. V. Astashkin, A. M. Raitsimring, T. K. Shokhireva and F. A. Walker, *J. Am. Chem. Soc.*, 2002, **124**, 6077–6089.
- 29 K. Tajima, K. Tada, J. Jinno, T. Edou, H. Mano, N. Azuma and K. Makino, *Inorg. Chim. Acta*, 1997, **254**, 29–35.
- 30 M. P. Jensen, M. Costas, R. Y. N. Ho, J. Kaizer, A. Mairata i Payeras, E. Münek, L. Que, Jr., J.-U. Rohde and A. Stubna, *J. Am. Chem. Soc.*, 2005, **127**, 10512–10525.
- 31 M. P. Jensen, A. M. I. Payeras, A. T. Fiedler, M. Costas, J. Kaizer, A. Stubna, E. Münek and L. Que, Jr., *Inorg. Chem.*, 2007, **46**, 2398–2408.
- 32 B. Shin, K. D. Sutherlin, T. Ohta, T. Ogura, E. I. Solomon and J. Cho, *Inorg. Chem.*, 2016, **55**, 12391–12399.
- 33 F. A. Chavez, C. V. Nguyen, M. M. Olmstead and P. K. Mascharak, *Inorg. Chem.*, 1996, **35**, 6282–6291.
- 34 Interestingly, the decay of **2** was facilitated by adding excess water in **2**, and a cobalt(II)-hydroxo complex was observed as a major peak in CSI-MS (Fig. S4–S6, ESI $\dagger$ ).
- 35 W. D. Bailey, N. L. Gagnon, C. E. Elwell, A. C. Cramblitt, C. J. Bouchey and W. B. Tolman, *Inorg. Chem.*, 2019, **58**, 4706–4711.